PHYSICAL REVIEW B VOLUME 6, NUMBER 6 15 SEPTEMBER 1972

Theoretical and Experimental Study of Raman Scattering from Coupled LO-Phonon-Plasmon Modes in Silicon Carbide†

Miles V. Klein and B. N. Ganguly
Department of Physics and Materials Research Laboratory, University of Illinois, Urbana, Illinois 61801

and

Priscilla J. Colwell*
Department of Physics, Northwestern University, Evanston, Illinois 60201
(Received 25 February 1972)

A general semiclassical derivation is given of the efficiency of the scattering of light from a longitudinal-optical (LO) phonon coupled to a single-component plasma in a semiconductor. The efficiency is the sum of two terms. One is due to the modulation of polarizability by atomic displacements and by the macroscopic longitudinal field; it obeys ordinary Raman polarization selection rules. The other term is due to free-electronic-charge-density fluctuations, is proportional to the square of the wave vector transferred, and obeys different selection rules. When the exciting light is near resonance with the band gap, the second term may have two interfering parts, one due to the free-electron-charge-density fluctuations and the other due to photon-induced, virtual, bound-electronic-charge-density fluctuations coupled to the macroscopic field (Fröhlich mechanism). New data are presented on coupled plasmon-phonon scattering in heavily nitrogen-doped (n-type) 6H silicon carbide. The plasmon is overdamped ($\omega_p\tau \approx 0.2$–0.3). The dominant light-scattering mechanism is shown to be the polarizability-modulation mechanism. The density mechanism is predicted to be 3500 times weaker. The ratio of polarizability derivatives in dimensionless form is $\gamma_{xxz} = +2.60$. From this and from published data on the nonlinear optical constants of 6H SiC we obtain the following value for the derivative of the polarizability with respect to relative atomic displacement: $\partial\alpha_{xy}/\partial u_z = (\mp 10.4 \pm 1.2) \times 10^{-16}\ \mathrm{cm}^2$. Absolute efficiencies are also calculated for the coupled mode spectrum in doped materials and for the A_1(LO) phonon in lightly doped crystals. Sum rules are derived for the differential efficiencies integrated with respect to the frequency squared.

I. INTRODUCTION

When the frequency of oscillation of a free-carrier plasma in a polar semiconductor is close to that of the longitudinal-optical (LO) phonon, the two excitations interact via their macroscopic electric fields. The resulting coupled modes have frequencies $\omega_\pm$ given by the zeros of the real part of the total dielectric constant.[1] The shape of the spectrum depends on the amount of plasmon damping due to scattering of the carriers[2] and on the nature of the experimental probe used to study the coupled modes.

A very effective probe is provided by inelastic scattering of light.[3] It occurs by means of three mechanisms[4]: the displacement mechanism, a modulation of the optical polarizability by the atomic displacements u (sometimes called the deformation-potential mechanism); the field mechanism, a modulation of the polarizability by the macroscopic longitudinal field $\mathcal{E}$ (sometimes called the electro-optic mechanism); and the density mechanism, a direct scattering by electronic-charge-density fluctuations ρ.

A derivation of the Raman efficiency due to all three effects will now be given. We will not make the usual separation of the resulting spectrum into ω_+ and ω_- components having frequency-dependent phonon and plasmon strengths.[5] Instead a direct calculation of the line shape for arbitrary plasmon damping strength will be given.

The case of large damping is of practical importance in wide-band-gap semiconductors. Heavily damped coupled modes have been observed in CdS,[6] GaP,[7] and SiC.[8,9] After a general discussion of the theoretical results, they will be used to analyze new data taken on heavily doped SiC. One of the fitting parameters will then be used to calculate two other parameters, one a ratio of polarizability derivatives, and the other a derivative of polarizability with respect to phonon displacement.

II. THEORY OF RAMAN SCATTERING FROM COUPLED PLASMON-PHONON MODES

A. Assumptions, Definitions, and Notation

It is assumed throughout most of this paper that the incident laser energy is far enough below the energy of the band gap that resonance effects can be neglected. In Appendix A there are some comments about the situation near resonance. Away from resonance we may use the notion of adiabatic modulation of the optical polarizability α by the phonon displacement u and by the field $\mathcal{E}$. The free

carriers will be assumed to be electrons for definiteness and will all be assumed to have the same reciprocal effective mass tensor $(m/m^*)_{ab}$. Thus, the discussion is restricted to a single-component plasma. A semiclassical argument[10] will be used to give the low-temperature Stokes scattering efficiency in terms of the rate of energy transferred to the medium by an effective external longitudinal driving field. This field will be screened self-consistently by use of appropriate susceptibilities. The resulting expressions are correct in the random-phase approximation.

The following definitions and notation will be used: $\vec{R}$, lattice site; $\vec{r}_j$, coordinate of the jth free electron; $\vec{k}_{1,2}$, incident and scattered photon wave vectors; $\omega_{1,2}$, incident and scattered photon frequencies; $\vec{\eta}_{1,2}$, incident and scattered photon polarization unit vectors (assumed real); $\omega = \omega_1 - \omega_2$, frequency of energy transfer; $\vec{q} = \vec{k}_1 - \vec{k}_2$, wave vector transferred; $\vec{\eta}_q = \vec{q}/|q|$, unit vector along $\vec{q}$ parallel to longitudinal displacements; $\eta_q^c u(\vec{R})$, cth Cartesian component of the longitudinal displacement within the unit cell at $\vec{R}$; $\eta_q^c \mathcal{E}(\vec{R})$, cth component of the longitudinal macroscopic electric field at $\vec{R}$; v_0, volume of a unit cell; V, volume of crystal; $\vec{E}(\vec{r})$, total transverse macroscopic field at optical frequencies; $\vec{A}(\vec{r})$, total optical vector potential; $r_0 = e^2/mc^2$, classical electron radius.

B. Derivation

The Hamiltonian will be the appropriate cross terms from

$$-\tfrac{1}{2}\sum_{R,a,b} E_a(\vec{R})\,\delta\alpha_{ab}(\vec{R})E_b(\vec{R}) + \tfrac{1}{2} r_0 \sum_{j,a,b} A_a(\vec{r}_j)(m/m^*)_{ab}A_b(\vec{r}_j) \quad ,$$

where

$$\delta\alpha_{ab}(\vec{R}) = \sum_c \left(\frac{\partial\alpha_{ab}}{\partial u_c}\,\eta_q^c u(\vec{R}) + \frac{\partial\alpha_{ab}}{\partial\mathcal{E}_c}\,\eta_q^c \mathcal{E}(\vec{R})\right)$$

is the first-order change in the polarizability of the Rth unit cell due to atomic displacements and the longitudinal field. The fields at optical frequencies are written

$$\vec{E}(\vec{R}) = \tfrac{1}{2}[\vec{\eta}_1 E_1 e^{i(\vec{k}_1\cdot\vec{R}-\omega_1 t)} + \vec{\eta}_2 E_2 e^{i(\vec{k}_2\cdot\vec{R}-\omega_2 t)} + \text{c.c.}] \quad ,$$

$$\vec{A}(\vec{r}_j) = (c/2i)[\vec{\eta}_1(E_1/\omega_1)e^{i(\vec{k}_1\cdot\vec{r}_j-\omega_1 t)} + \vec{\eta}_2(E_2/\omega_2)e^{i(\vec{k}_2\cdot\vec{r}_j-\omega_2 t)}] + \text{c.c.} \quad .$$

The Hamiltonian involves the $E_1E_2^*$ cross terms and is

$$H' = -\tfrac{1}{4}E_1E_2^* e^{-i\omega t}\left(\frac{\partial\alpha}{\partial u}\,u_q^* + \frac{\partial\alpha}{\partial\mathcal{E}}\,\mathcal{E}_q^* - \frac{r_0c^2m}{\omega_1\omega_2 m^*}\,\rho_q^{e*}\right) + \text{H.c.} \quad , \qquad (1a)$$

where

$$\frac{\partial\alpha}{\partial u} \equiv \sum_{a,b,c} \eta_1^a\eta_2^b\eta_q^c \frac{\partial\alpha_{ab}}{\partial u_c} \quad , \qquad (1b)$$

$$\frac{\partial\alpha}{\partial\mathcal{E}} \equiv \sum_{a,b,c} \eta_1^a\eta_2^b\eta_q^c \frac{\partial\alpha_{ab}}{\partial\mathcal{E}_c} \quad , \qquad (1c)$$

$$\frac{m}{m^*} \equiv \sum_{a,b} \eta_1^a\eta_2^b\left(\frac{m}{m^*}\right)_{ab} \quad , \qquad (1d)$$

$$u_q^* \equiv \textstyle\sum_{\vec{R}} u(\vec{R})e^{i\vec{q}\cdot\vec{R}} \quad , \qquad (1e)$$

$$\mathcal{E}_q^* \equiv \textstyle\sum_{\vec{R}} \mathcal{E}(\vec{R})e^{i\vec{q}\cdot\vec{R}} \quad , \qquad (1f)$$

$$\rho_q^* \equiv \textstyle\sum_j e^{i\vec{q}\cdot\vec{r}_j} \quad , \qquad (1g)$$

and H.c. stands for Hermitian conjugate.

The phonon displacement and the electron density produce ionic and electronic contributions to the qth Fourier component of the polarization

$$P_q = P_q^e + P_q^i \qquad (2a)$$

with

$$P_q^i = e^* u_q/V \quad , \qquad (2b)$$

$$P_q^e = e\rho_q^e/Viq \quad . \qquad (2c)$$

Here e^* is the effective charge associated with the displacement u.

The polarization from ions and conduction electrons will be screened by the bound electrons, producing a macroscopic longitudinal electric field with Fourier component

$$\mathcal{E}_q = -4\pi P_q V/v_0\epsilon_\infty \quad . \qquad (3)$$

This expression is then used to eliminate $\mathcal{E}_q$ from Eqs. (1). The Hamiltonian may thus be written in terms of $P_q^{i,e}$ in the form

$$H' = -\tfrac{1}{4}E_1E_2^* e^{-i\omega t} V \sum_{j=i,e} d_j P_q^{j*} + \text{H.c.} \qquad (4a)$$

or

$$H' = -V\textstyle\sum_j D_j P_q^{j*} + \text{H.c.} \qquad (4b)$$

The last equality defines the effective driving fields $D_{i,e}$ in terms of the reduced fields $d_{i,e}$, which are given by

$$d_i = d_i' + id_i'', \quad \text{with } d_i' = d_u + d_{\mathcal{E}}, \quad d_i'' = 0 \qquad (5a)$$

$$d_e = d_e' + id_e'', \quad \text{with } d_e' = d_{\mathcal{E}}, \quad d_e'' = d_\rho \quad . \qquad (5b)$$

Here

$$d_u = \frac{1}{e^*}\frac{\partial\alpha}{\partial u} \quad , \qquad (6a)$$

$$d_{\mathcal{E}} = -\frac{4\pi}{\epsilon_\infty v_0}\frac{\partial\alpha}{\partial\mathcal{E}} \quad , \qquad (6b)$$

$$d_\rho = \frac{r_0c^2mq}{\omega_1\omega_2 m^* e} \quad . \qquad (6c)$$

The driving fields $D_{i,e}$ act on the ionic and electronic subsystems. In the random-phase approxi-

mation the Coulomb interaction within and between the subsystems is taken into account by allowing them to respond linearly to the total effective fields

$$D_{i,e} - 4\pi \langle P_q \rangle / \epsilon_\infty$$

to induce the polarizations

$$\langle P_q^{i,e} \rangle = \chi_{i,e}(D_{i,e} - 4\pi \langle P_q \rangle / \epsilon_\infty) \quad , \tag{7}$$

where χ_i and χ_e are the susceptibilities of the ionic and free electronic systems for $(\vec{q}, \omega)$ Fourier components. For small q and for frequencies in the plasmon regime they are given by

$$4\pi\chi_i = \frac{\omega_l^2 - \omega_t^2}{\omega_t^2 - \omega^2} \epsilon_\infty \quad , \tag{8a}$$

$$4\pi\chi_e = -\frac{\omega_p^2 \epsilon_\infty}{\omega(\omega + i\Gamma)} \quad . \tag{8b}$$

Here ω_p, ω_l, and ω_t are the frequencies of the plasmon, LO phonon, and transverse-optical (TO) phonon, respectively. Γ is the plasmon damping factor and equals the reciprocal of the electron scattering time.

The solutions to Eqs. (7) are

$$\langle P_q^j \rangle = \sum_{j'} \chi_{jj'} D_{j'} \quad , \tag{9a}$$

with

$$\chi_{jj'} \equiv \chi_j \delta_{jj'} - 4\pi \chi_j \chi_{j'} / \epsilon \quad , \tag{9b}$$

where ϵ is the total dielectric constant

$$\epsilon = \epsilon_\infty + 4\pi\chi_i + 4\pi\chi_e \quad . \tag{10}$$

The effective driving fields $D_{i,e}$ will transfer power to the medium as follows:

$$P = 2\omega V \operatorname{Im} \sum_{jj'} D_j^* \chi_{jj'} D_{j'}$$

$$= \omega |E_1|^2 |E_2|^2 V \operatorname{Im} \sum_{jj'} \tfrac{1}{8} d_j^* \chi_{jj'} d_{j'} \quad . \tag{11}$$

$P_s^{(1)}$, the power scattered into a single mode of the Raman field, is related to the power transferred to the medium by

$$P_s^{(1)} = \omega_2 P / \omega \quad . \tag{12}$$

The total power of a given polarization scattered into solid angle $d\Omega$ and frequency range $d\omega_2$ is

$$P_s^{(\mathrm{tot})} = P_s^{(1)} \frac{V}{8\pi^3} \left(\frac{n_2}{c}\right)^3 \omega_2^2 \, d\omega_2 d\Omega \quad , \tag{13}$$

where n_2 is the refractive index of the medium at frequency ω_2.

The magnitude of the field strength $|E_1|$ is given in terms of the incident power P_i by

$$|E_1|^2 = 8\pi P_i / n_1 c A \quad , \tag{14}$$

where A is the cross-sectional area of the incident laser beam. The field strength E_2 for a low-temperature Stokes process is that associated with a single mode containing one quantum per unit volume, i.e., the zero-point field, and obeys

$$|E_2|^2 = 8\pi\hbar\omega_2 / n_2^2 V \quad . \tag{15}$$

The volume V is written LA, where L is the length of sample illuminated by the laser beam.

The differential Raman efficiency is then given by

$$\frac{d^2R}{d\omega\, d\Omega} = \frac{P_s^{(\mathrm{tot})}}{P_i L \, d\omega_2 \, d\Omega} = \left(\frac{\omega_2}{c}\right)^4 \frac{\hbar n_2}{\pi n_1} \operatorname{Im} \sum_{jj'} d_j^* \chi_{jj'} d_{j'} \quad . \tag{16}$$

The assumption that both d_i and d_e are complex leads to

$$\Sigma(\omega) \equiv \sum_{jj'} \operatorname{Im} d_j^* \chi_{jj'} d_{j'} = \sum_{jj'} (d_j' d_{j'}' + d_j'' d_{j'}'') \operatorname{Im} \chi_{jj'}$$

$$= \frac{(\operatorname{Im}\chi_e)\epsilon_\infty^2}{|\epsilon|^2 (\omega_t^2 - \omega^2)^2} \left[d_e'^2 (\omega_0'^2 - \omega^2)^2 + d_e''^2 (\omega_0''^2 - \omega^2)^2 \right] \quad , \tag{17}$$

where new frequencies have been introduced by

$$\omega_0'^2 = \omega_t^2 - (\omega_l^2 - \omega_t^2)(d_i' - d_e')/d_e' \tag{18a}$$

or

$$\omega_0'^2 = \omega_t^2 [\epsilon_0 - (\epsilon_0 - \epsilon_\infty)(d_i'/d_e')]/\epsilon_\infty \tag{18b}$$

with an analogous expression for ω_0''. In Eq. (18b) we have used the Lyddane-Sachs-Teller relation $\omega_l^2/\omega_t^2 = \epsilon_0/\epsilon_\infty$. The factor multiplying the brackets in the expression (17) for Σ is readily evaluated as

$$\omega_p^2 \epsilon_\infty \omega\Gamma / 4\pi\Delta$$

with

$$\Delta = [\omega^2(\omega_l^2 - \omega^2) - \omega_p^2(\omega_t^2 - \omega^2)]^2 + \omega^2\Gamma^2(\omega_l^2 - \omega^2)^2 \quad . \tag{19a}$$

The zeros of the expression in square brackets in Eq. (19a) define the frequencies $\omega_\pm$ of the coupled modes. Thus an alternate form for Δ is

$$\Delta = (\omega^2 - \omega_+^2)^2 (\omega^2 - \omega_-^2)^2 + \omega^2\Gamma^2(\omega_l^2 - \omega^2)^2 \quad . \tag{19b}$$

This gives

$$\Sigma(\omega) = \omega_p^2 \epsilon_\infty \omega\Gamma [d_e'^2 (\omega_0'^2 - \omega^2)^2 + d_e''^2 (\omega_0''^2 - \omega^2)^2] / 4\pi\Delta . \tag{20}$$

C. Discussion of the Derived Expressions

From Eqs. (16) and (17) we see that the important frequency dependence of the Raman efficiency is that of $\Sigma(\omega)$, which consists of the sum of two noninterfering terms. The first term is due to the combination of u and $\mathcal{E}$ mechanisms. It obeys the usual polarization selection rules for LO phonons that follow from the condition that $\partial\alpha/\partial u$ and $\partial\alpha/\partial\mathcal{E} \neq 0$.[11] Its contribution to the Raman efficiency is

$$\left(\frac{d^2R}{d\omega\, d\Omega}\right)_{u,\mathcal{E}} = \left(\frac{4\pi}{\epsilon_\infty v_0} \frac{\partial\alpha}{\partial\mathcal{E}}\right)^2 \frac{\hbar n_2}{\pi n_1} \left(\frac{\omega_2}{c}\right)^4$$

$$\times\left[\frac{\omega_p^2\epsilon_\infty}{4\pi}\ \frac{\omega\Gamma(\omega_0'^2-\omega^2)^2}{\Delta}\right], \quad (21)$$

with

$$\omega_0'^2=\omega_t^2-d_u(\omega_l^2-\omega_t^2)d_{\mathcal{E}}^{-1} \quad (22a)$$

or

$$\omega_0'^2=\omega_t^2+\frac{e^*}{M}\frac{\partial\alpha/\partial u}{\partial\alpha/\partial\mathcal{E}} \quad (22b)$$

or

$$\omega_0'^2=\omega_t^2+\left(\frac{\epsilon_0-\epsilon_\infty}{4\pi M}\right)^{1/2}\omega_t\frac{\partial\alpha/\partial u}{\partial\alpha/\partial\mathcal{E}}v_0^{1/2}. \quad (22c)$$

Here M is the reduced mass corresponding to the coordinate u. This result has the same form as that given by Mooradian and McWhorter[4] for the special case of the zinc-blende structure. Note that the scattering is zero when $\omega=\omega_0'$. An experimental determination of the position of this zero will yield a value for the ratio $(\partial\alpha/\partial u)/(\partial\alpha/\partial\mathcal{E})$ by use of Eq. (22b) or (22c).[12]

In the ordinary situation below resonance $d_i''=0$ and $d_e''=d_\rho$. Then $\omega_0'^2=\omega_l^2$, and the contribution of the density mechanism to the Raman efficiency is

$$\left(\frac{d^2R}{d\omega d\Omega}\right)_\rho=\left(\frac{mr_0qc^2}{m^*e\omega_1\omega_2}\right)^2\frac{\hbar n_2}{\pi m_1}\left(\frac{\omega_2}{c}\right)^4\times\left[\frac{\omega_p^2\epsilon_\infty}{4\pi}\ \frac{\omega\Gamma(\omega_l^2-\omega^2)^2}{\Delta}\right]. \quad (23)$$

This is distinguishable from the $u,\mathcal{E}$ contribution [Eq. (21)] by a generally different quantitative value and by three qualitative features: (a) a dependence on q^2—thus there should be no contribution in the forward scattering case where $q\approx 0$; (b) a zero at $\omega^2=\omega_l^2$ instead of at $\omega^2=\omega_0'^2$; (c) polarization selection rules governed by

$$m/m^*=\vec{\eta}_1\cdot(\overleftrightarrow{m}/m^*)\cdot\eta_2$$

instead of by

$$\frac{\partial\alpha}{\partial\mathcal{E}}=\sum_c\vec{\eta}_1\cdot(\partial\overleftrightarrow{\alpha}/\partial\mathcal{E}_c)\cdot\vec{\eta}_2\eta_q^c.$$

These distinguishing features should make possible a clear experimental determination of the mechanism responsible for light scattering from the coupled modes.

An expression sometimes proposed to describe the coupled mode line shape is[8,9]

$$-\frac{1}{4\pi}\,\mathrm{Im}\frac{1}{\epsilon}=\frac{\mathrm{Im}\chi_e}{|\epsilon|^2}=\frac{\omega_p^2\omega\Gamma}{4\pi\epsilon_\infty}\ \frac{\omega_t^2-\omega^2}{\Delta}. \quad (24)$$

This gives an incorrect result for the case of strong damping ($\Gamma\gtrsim\omega_p$). For then Δ is relatively slowly varying, and the zero of Eq. (24) at $\omega=\omega_t$ would be distinguishable from those of Eqs. (21) and (22) at $\omega=\omega_0'$ and $\omega=\omega_l$. The correct scattering efficiency would be proportional to Eq. (24) if the coupling of the optical radiation fields were only to the total charge density $-e\rho_q^e+e^*\rho_q^i$ or to the total longitudinal polarization P_q. This would be the case for the combined $(u,\mathcal{E})$ mechanism if $\partial\alpha/\partial u=0$. This will not be the case for the density mechanism, since the A^2 term in the Hamiltonian couples essentially only to electronic-charge-density fluctuations; the amplitude of the direct coupling to ionic-charge-density fluctuations is less by the ratio of the electron mass to the ion mass.

There is the possibility of qualitatively different effects occurring near resonance. This is discussed in Appendix A.

III. EXPERIMENT

A. Introduction

The 6*H* polytype of SiC has six molecules per unit cell. The only optical phonons with appreciable macroscopic electric fields are those in which the two atoms in each molecule undergo the same relative displacement u. These phonons have only a small A_1-E_1 anisotropy shift and have almost the same frequency as the LO phonon in cubic SiC.[13]

There is a multivalley conduction band in 6*H* SiC. The minima are along the lines ML in the Brillouin zone.[8,9] The zone is the same as that for a simple hexagonal lattice, and the lines ML are the intersections of the mirror planes with the rectangular zone faces. There are three different groups of electrons in these valleys. The effective mass ellipsoids for each group will all have the same principal axis in the z (or c) direction. Another principal axis will be along [1000], [0100], or [0010]. The data to be discussed below concern coupled modes of A_1 symmetry where the electronic and lattice displacements are along the z axis. The effective mass entering the expression for the plasma frequency

$$\omega_p^2=4\pi ne^2/m_{eff}\epsilon_\infty$$

is $m/m_{eff}=(m/m^*)_{zz}$ and is the same for the three groups of electrons. As far as the $(u,\mathcal{E})$ mechanism for light scattering is concerned, the three groups behave as a single-component plasma. Each group of electrons has different values for xx, xy, and yy components of $\overleftrightarrow{m}/m^*$. This means that in general each group will have its own value of m/m^* appearing in Eqs. (1). These equations and the subsequent derivations must be generalized to treat the three groups separately when the ρ mechanism is being discussed.[14]

We have previously presented the results of a study of Raman scattering by electronic excitations in 6*H* SiC doped with nitrogen donors.[8,9] In a sample with a nominal doping of $6\times10^{19}/\mathrm{cm}^3$ a very broad asymmetric line was observed having

TABLE I. Position and width of some optical phonons in 6*H* SiC (wave number in cm^{-1}).

Nitrogen doping (cm^{-3})	Temp. (K)	A_1(LO) Position	A_1(LO) Width[a]	A_1(TO) Position	A_1(TO) Width[a]	E_2 Position	E_2 Width[a]	E_2 Position	E_2 Width[a]
1×10^{17}	12	967.0	3.2	788.8	2	769.0	2	789.6	2
1×10^{17}	300	965.0	4			767.7	2.7	788.3	2.7
6×10^{19}	110					769.0	2.6	789.6	2.6
1×10^{17}	300	964[b]		788[b]		766[b]		788[b]	

[a]Widths are uncorrected for the instrumental slit width of 1.2 cm^{-1}.

[b]Data from Ref. 13.

a peak at about 980 cm^{-1} in the general vicinity of the A_1(LO) phonon. An approximate fit was made using the imaginary part of the reciprocal of the dielectric constant [Eq. (24)]. The calculated curve fit the data well near the peak and at higher frequencies, but the data points dropped sharply below the computed curve below 960 cm^{-1}. The fitting parameters were $\omega_p = 700$ cm^{-1} and $\omega_p\tau = 0.29$, corresponding to an extreme case of overdamping.

B. Techniques

Additional data were gathered to provide a test of the theoretical expressions discussed above. Backscattering experiments were performed on both *a* and *c* surfaces [$\bar{x}(yy)x$ and $\bar{z}(yy)z$ geometries] of the same 6×10^{19} sample studied previously. From the *a* surface no structure was observed that could correspond to coupled E_1(LO)-plasmon modes. Coupling to such modes would have been via the ρ mechanism since with $\bar{x}(yy)x$ ordinary selection rules give no coupling to LO. From this negative result and the positive result on the *c* surface [where A_1(LO) is allowed by ordinary selection rules], we conclude by a small extrapolation that the ρ mechanism yields much weaker scattering than the $(u, \mathcal{E})$ mechanism. This conclusion is supported by numerical calculations given below.

The data were taken using approximately 1 W of 4880-Å laser light focussed to a circular spot 150 mμ in diameter. The beam caused heating of the sample, even when it was cooled directly by a stream of cold helium gas in a variable-temperature Dewar. The sample temperature was raised from the 12 K of its surroundings, as determined by a thermocouple, to 110 K, as determined by the ratio of anti-Stokes–to–Stokes Raman intensity of the close-in electronic Raman continuum.[8,9] Additional measurements were taken with the sample at room temperature.

We calibrated the wave-number scale for the Raman runs by use of a neon lamp and published calibrated data.[15] Neon lines were also used to determine the positions of several other phonon peaks in the 6×10^{19} sample and in the "nominally pure" (1×10^{17} donors/cm^3) sample studied previously.[9]

C. Results

Peak positions and widths for the several phonons are given in Table I and are accurate to within 0.3 cm^{-1}. They are compared with earlier published data taken at room temperature.[13] The nitrogen doping did not affect the peak position of the A_1(TO) and high-frequency E_2 phonons, but it did broaden the lines slightly.

Data from the heavily doped sample in the region of the coupled LO phonon-plasmon mode are shown in Fig. 1. Also shown are fits using Eq. (21) superimposed on a decreasing linear base line. The parameters used for the fits are given in Table II. Owing to the large damping, the spectrum does not give peaks near ω_+ and ω_-; these parameters would have the values 1060 and 490 cm^{-1} for $\omega_p = 660$ cm^{-1}. Over a certain range

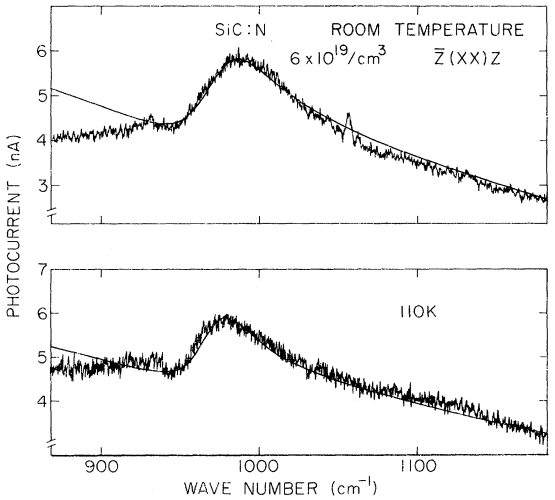

FIG. 1. Coupled-mode spectrum at two different temperatures. Solid line is calculated from Eq. (21) using the parameters of Table II. Linearly decreasing background terms have been added to fit the high-frequency region.

TABLE II. Parameters used to fit Eq. (21) to Raman data in Fig. 1 (wave number in cm^{-1}).

Temp. (K)	ω_l	ω_t	ω_0'	ω_p	Γ	$\omega_p\tau$	$\tau(10^{-15}$ sec)
110	967	789	928	660	3400	0.19	1.55
300	965	787	928	620	2200	0.28	2.4

one can vary ω_p and Γ without affecting the goodness of the fit—it is only necessary to keep ω_p^2/Γ constant. For instance, the room-temperature curve may be fit equally well with $\omega_p = 660$, $\Gamma = 2500$ as with $\omega_p = 620$, $\Gamma = 2200$. The quality of the fit is quite sensitive to the value of ω_0', however. The calculated curves do not reproduce the small peak at 930 cm^{-1}; we attribute that to an impurity effect of undetermined origin.

There is a slowly varying "base line" on which the phonon-plasmon coupled mode is superimposed. Part of this appears in the $\bar{z}(xy)z$ (E_2-only) spectrum. This E_2 continuum interferes somewhat with the 790-cm^{-1} E_2 phonon, but this interference is not as strong as the ones observed between lower-frequency E_2 phonons and electronic excitations described previously.[8,9]

There is additional background in the $\bar{z}(xx)z$ data of Fig. 1 (where A_1 and E_2 symmetries are allowed) beyond what is observed in the E_2-only data. Thus the "background" apparently has an A_1 component. It is broad and structureless, peaking near 930 cm^{-1}. The various contributions to the background have made it difficult to obtain better fits in the regions away from the peak than those shown in Fig. 1.

D. Discussion of the Experimental Results

One of the theoretical curves used in Fig. 1 is shown over a wider frequency range without the linear base line in the upper curve of Fig. 2. This represents the contribution of the $(u, \mathcal{E})$ mechanism as given by Eq. (21). As mentioned above, for the ρ mechanism in this multivalley material, one should really treat a multicomponent plasma. Since we do not know how anisotropic the effective mass tensors are, we cannot do a quantitative calculation. Therefore, in the lower curve we give the predictions of the single-component theory of Eq. (23) for the ρ mechanism using the same parameters as those used for the upper curve. Shifting the zero from $\omega_0' = 928$ cm^{-1} to $\omega_l = 965$ cm^{-1} has a strong effect on the shape of the spectrum, producing a dip at ω_l rather than a real high-frequency peak. There is also a large quantitative difference; estimates below indicate that the maximum in the upper curve of Fig. 2 is 3500 times higher than the upper maximum in the lower curve.

Both parts of Fig. 2 show a very strong, broad, distorted "ω_-" peak. (Recall that $\omega_- = 490$ cm^{-1}.) We were not able to observe this experimentally because of the strong-low-frequency scattering from broadened valley-orbit transitions.[8,9]

The fitted value of ω_0' will give a value for the dimensionless parameter γ used by Scott, Damen, and Shah[12]:

$$\gamma = \frac{\omega_t^2}{\omega_0'^2 - \omega_t^2} = M\omega_t^2 \frac{\partial\alpha/\partial\mathcal{E}}{e^*\partial\alpha/\partial u} . \tag{25a}$$

More specifically, the present experiment with its $\bar{z}(xx)z$ geometry measures

$$\gamma_{xxz} = M\omega_t^2 \frac{\partial\alpha_{xx}/\partial\mathcal{E}_z}{e^*\partial\alpha_{xx}/\partial u_z} . \tag{25b}$$

Our results for 6*H* SiC give

$$\gamma_{xxz} = +2.60 . \tag{25c}$$

This has the same sign and nearly the same value as that found in several II-VI compounds having the wurtzite structure (2*H*).[12]

The nonlinear optical constants of 6*H* SiC have recently been measured.[16] The parameter of interest to us is d_{15} which appears in the following expression for the optical polarization vector at the second harmonic frequency

$$P_x(2\omega) = 2d_{15}E_x(\omega)E_z(\omega) . \tag{26}$$

Neglecting dispersion of d_{15}, we may apply Eq. (26) to our case in the form

$$P_x(\omega_1 - \omega_l) = 2d_{15}E_x(\omega_1)\mathcal{E}_z(\omega_l) \tag{27}$$

and find that

$$\frac{1}{v_0}\frac{\partial\alpha_{xx}}{\partial\mathcal{E}_z} = 2d_{15} . \tag{28}$$

The numerical result from Ref. 16 gives

$$\frac{1}{v_0}\frac{\partial\alpha}{\partial\mathcal{E}} = 2(\mp 9.1 \pm 1)\times 10^{-12} \text{ m/V}$$
$$= \mp(54.6 \pm 11\%)\times 10^{-8} \text{ cm/stat V} . \tag{29}$$

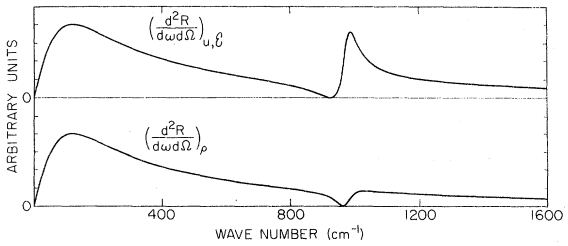

FIG. 2. Raman efficiencies calculated according to Eqs. (21) and (23) using the room-temperature parameters from Table II. Numerical values at the peaks are given in Eqs. (33) and (35). Proper relative efficiencies are obtained if the lower curve is reduced by a factor of about 800.

When this value is used with Eqs. (25b) and (25c) we find

$$\frac{\partial \alpha_{xx}}{\partial u_z} = (\mp 10.4 \pm 1.2) \times 10^{-16} \text{ cm}^2 . \quad (30)$$

To obtain this result we used[16]

$$\epsilon_\infty = 6.56 , \quad (31)$$

$$v_0 = 2.075 \times 10^{-23} \text{ cm}^3 . \quad (32)$$

We assume that v_0 is one-sixth of the unit cell volume.

It is now possible to make quantitative calculations of the $(u, \mathcal{E})$ and ρ contributions to the Raman efficiency. Using the room-temperature parameters from Table II, appropriate for Fig. 2, we find that the expression in large square brackets in Eq. (21) has a peak value of 0.32 at 990 cm^{-1}. Using this and the result from Eq. (29) we find

$$\left(\frac{d^2R}{d\omega d\Omega}\right)_{u,\mathcal{E}} (\omega = 990 \text{ cm}^{-1}) = 2.6 \times 10^{-20} \text{ sec/cm sr} . \quad (33)$$

Guessing the effective width of the upper part of the $(u, \mathcal{E})$ curve of Fig. 2 as 2×10^{14} sec^{-1} (1060 cm^{-1}), we then obtain this rough estimate of the total efficiency in the high-frequency region

$$\left(\frac{dR}{d\Omega}\right)_{u,\mathcal{E}} \sim 5 \times 10^{-6} \text{ cm}^{-1} . \quad (34)$$

The expression in large square brackets in Eq. (23) has a local maximum value of 0.088 at 1036 cm^{-1}. Using this result in Eq. (23) with $m^*/m = \frac{1}{2}$ we find

$$\left(\frac{d^2R}{d\omega d\Omega}\right)_{\rho} (\omega = 1036 \text{ cm}^{-1}) = 0.75 \times 10^{-23} \text{ sec/cm sr} . \quad (35)$$

This is 3500 times smaller than the upper-peak value due to the $(u, \mathcal{E})$ mechanism. Equations (33) and (35) then give the absolute scale of peak heights in Fig. 2.

It is also possible to use Eq. (29) in Eq. (21) in the limit of small ω_p and small Γ. As ω_p and Γ tend to zero, we find that the term in large square brackets in Eq. (21) tends to a δ function with an integrated strength

$$\frac{\omega_p^2 \epsilon_\infty}{4\pi} \int_0^\infty \frac{\omega \Gamma (\omega_0'^2 - \omega^2)^2 d\omega}{\Delta} \rightarrow \frac{\epsilon_\infty}{8} \frac{(\omega_0'^2 - \omega_t^2)^2}{\omega_t (\omega_l^2 - \omega_t^2)} . \quad (36)$$

This then gives the integrated scattering efficiency for the A_1(LO) phonon in the (xx) geometry at 4880 Å as

$$\left(\frac{dR}{d\Omega}\right)_{A_1(\text{LO})} = 2.1 \times 10^{-7} \text{ cm}^{-1} . \quad (37)$$

There are more general expressions for the scattering efficiency integrated over ω^2 rather than ω. They are derived in Appendix B.

IV. SUMMARY AND CONCLUDING REMARKS

A derivation of the scattering efficiency from the coupled modes has been given from a unified point of view. We found no interference between the ρ mechanism and the $(u, \mathcal{E})$ mechanism. The reason for this can be most easily seen when the ρ coupling term in the Hamiltonian is expressed in terms of the electronic polarization, for then a factor of i introduces a 90° phase shift. The possibility of an additional mechanism that may interfere with the ρ mechanism is discussed in Appendix A.

As noted by other workers, the u and $\mathcal{E}$ mechanisms interfere to produce a minimum at a frequency ω_0' that depends on the ratio $(\partial\alpha/\partial\mathcal{E})/(\partial\alpha/\partial u)$. Data on 6$H$ SiC doped with 6×10^{19} nitrogen-donor atoms/cm^3 were fit using the calculated formula for the $(u, \mathcal{E})$ mechanism. (The ρ mechanism was found experimentally to be too weak to detect.) The fitted value of ω_0' gave a dimensionless polarizability ratio close to that found for other hexagonal materials. The calculated value of $|\partial\alpha/\partial u| \approx 10^{-15}$ cm^2 is about what one would expect. The calculated value of the peak-differential Raman efficiency given by Eq. (33) may be used as an internal standard of absolute efficiency with which to compare the various other peaks observed with the same heavily doped sample. Similarly the value for the total efficiency given in Eq. (37) may be used as an internal-calibration standard for lightly doped samples.

The effect of adding the heavily damped "free" carriers has been to shift the LO peak from 965 cm^{-1} to a very asymmetric peak at 990 cm^{-1}. The addition of the carriers has also increased the scattering efficiency integrated over ω in the high-frequency region from 2.1×10^{-7} cm^{-1} to about 5×10^{-6} cm^{-1}. This is qualitatively consistent with the sum rule of Eq. (46) in Appendix B, which involves a total integral of the scattering efficiency over ω^2.

APPENDIX A: PLASMON-PHONON COUPLING NEAR RESONANCE

The above semiclassical derivation must be put on an explicit quantum-mechanical basis when the laser energy is close to the band gap. Many of the formulas will carry over provided that the appropriate resonant-energy factors are inserted into m/m^*, $\partial\alpha/\partial u$, and $\partial\alpha/\partial\mathcal{E}$.[17]

Near resonance a qualitatively new scattering mechanism becomes important.[18] It results from intraband matrix elements of H_F, the Fröhlich interaction, between intermediate states created by the virtual absorption of a laser photon. In the language of the present paper, H_F is simply the Coulomb interaction between the total charge-den-

sity operator ρ_q used above and ρ_q^{be}, the density operator for the bound charge created by the absorption of the virtual photon. The result of using H_F in a third-order perturbation calculation is essentially to add a term to the effective Hamiltonian in Eqs. (4a) and (4b) that is large only near resonance and proportional to $iq(P_q^i + P_q^e)$. This would introduce an extra term d_F proportional to q and containing an inner product of the phonon polarization vectors $\vec{\eta}_1$, $\vec{\eta}_2$ with a tensor having the full symmetry of the crystal. Thus in Eqs. (5) we would have

$$d_t'' = d_F , \tag{38a}$$

$$d_e'' = d_\rho + d_F . \tag{38b}$$

We note that when the effective-mass tensor has the full symmetry of the crystal, d_ρ and d_F will both yield the same polarization and wave-vector selection rules. If the Fröhlich mechanism is dominant, the optical radiation fields couple only to $(P_q^i + P_q^e)$. The Raman efficiency will then be proportional to $\mathrm{Im}\epsilon^{-1}$, which has a zero at ω_t.

If the resonant-energy denominators are such that d_ρ and d_F are of comparable magnitude, there will be an interference between scattering by the ρ mechanism and by the F mechanism. This will contribute to the scattering efficiency a term obtainable from Eqs. (16)–(18):

$$\left(\frac{d^2R}{d\omega\, d\Omega}\right)_{\rho,F} = \left(\frac{\omega_2}{c}\right)^4 \frac{\hbar n_2}{\pi m_1} \frac{\mathrm{Im}\chi_e}{|\epsilon|^2} \frac{d_e''^2(\omega_0''^2 - \omega^2)^2}{(\omega_t^2 - \omega^2)^2} , \tag{39a}$$

with

$$\omega_0''^2 = \omega_t^2 + (\omega_l^2 - \omega_t^2) d_\rho/(d_\rho + d_F) . \tag{39b}$$

Thus as resonance conditions change to make d_ρ/d_F vary from $\gg 1$ to $\ll 1$, the parameter $\omega_0''^2$ should vary from ω_l^2 to ω_t^2. This will give a line shape to the coupled-mode spectrum that depends on the resonant enhancement of d_F relative to d_ρ.

APPENDIX B: SUM RULES AND INTEGRATED EFFICIENCIES

We will now derive expressions for integrals of the form

$$\int_0^\infty \frac{d^2R}{d\omega\, d\Omega}\, 2\omega\, d\omega = \int_0^\infty \frac{d^2R}{d\omega\, d\Omega}\, d\omega^2 .$$

These will be independent of the plasmon damping factor Γ.

The derivation follows from a dispersion relation[19]

$$P\int_0^\infty \frac{\mathrm{Im}\chi_{jj'}(\omega')\, d\omega'}{\omega' - \omega} = \pi \mathrm{Re}\chi_{jj'}(\omega) .$$

Use is then made of the fact that $\mathrm{Im}\chi(-\omega') = -\mathrm{Im}\chi(\omega')$ to obtain for large ω

$$\int_0^\infty \frac{\mathrm{Im}\chi_{jj'}(\omega')\, 2\omega'\, d\omega'}{\omega'^2 - \omega^2} = \pi \mathrm{Re}\chi_{jj'}(\omega)$$

or

$$\int_0^\infty \mathrm{Im}\chi_{jj'}(\omega')\, 2\omega'\, d\omega' = -\lim_{\omega\to\infty} \pi\omega^2 \chi_{jj'}(\omega) . \tag{40}$$

With the help of Eqs. (8), (9b), and (10) we find

$$\int_0^\infty \mathrm{Im}\chi_{jj'}(\omega)\, 2\omega\, d\omega = \tfrac{1}{4}\delta_{jj'}\epsilon_\infty \omega_j^2 , \quad \text{for } j = i, e \tag{41a}$$

where

$$\omega_i^2 = \omega_l^2 - \omega_t^2 , \tag{41b}$$

$$\omega_e^2 = \omega_p^2 . \tag{41c}$$

This allows us to integrate the quantity $\Sigma(\omega)$ appearing in Eq. (17) to obtain

$$\int_0^\infty \Sigma(\omega) 2\omega\, d\omega = \tfrac{1}{4}\epsilon_\infty [(d_i'^2 + d_i''^2)(\omega_l^2 - \omega_t^2) + (d_e'^2 + d_e''^2)\omega_p^2] . \tag{42}$$

Note that this is independent of Γ.

Equations (5) and (42) may then be used to obtain an integral of the quantity in the large square brackets in Eq. (21):

$$\frac{\omega_p^2 \epsilon_\infty}{4\pi} \int_0^\infty \frac{2\omega^2 \Gamma(\omega_0'^2 - \omega^2)^2 d\omega}{\Delta} = \frac{\epsilon_\infty}{4}\left(\frac{(\omega_0'^2 - \omega_t^2)^2}{\omega_l^2 - \omega_t^2} + \omega_p^2\right) . \tag{43}$$

This result is consistent with Eq. (36). We also obtain an integral of the quantity in the large square brackets in Eq. (23) as follows:

$$\frac{\omega_p^2 \epsilon_\infty}{4\pi} \int_0^\infty \frac{2\omega^2 \Gamma(\omega_l^2 - \omega^2)^2 d\omega}{\Delta} = \frac{\epsilon_\infty \omega_p^2}{4} . \tag{44}$$

Equations (43) and (44) then give the Raman sum rules

$$\int_0^\infty \left(\frac{d^2R}{d\omega\, d\Omega}\right)_{u,\mathcal{E}} 2\omega d\omega = \left(\frac{4\pi}{\epsilon_\infty v_0} \frac{\partial\alpha}{\partial\mathcal{E}}\right)^2 \frac{\hbar}{\pi} \frac{n_2}{n_1} \left(\frac{\omega_2}{c}\right)^4 \times \frac{\epsilon_\infty}{4}\left(\frac{(\omega_0'^2 - \omega_l^2)^2}{\omega_l^2 - \omega_t^2} + \omega_p^2\right) , \tag{45}$$

$$\int_0^\infty \left(\frac{d^2R}{d\omega\, d\Omega}\right)_\rho 2\omega\, d\omega = \left(\frac{m r_0 q c^2}{m^* e \omega_1 \omega_2}\right)^2 \frac{\hbar}{\pi} \frac{n_2}{n_1} \times \left(\frac{\omega_2}{c}\right)^4 \frac{\epsilon_\infty \omega_p^2}{4} . \tag{46}$$

These results are independent of plasmon damping and show clearly how the integrated Raman strength increases with increasing electron density (increasing ω_p^2).

For completeness we also give expressions for several integrated scattering efficiencies. For LO phonons in the absence of free electrons we set $\omega_p = 0$ in Eq. (45) and multiply by $\frac{1}{2}\omega_l$ to obtain

$$\left(\frac{dR}{d\Omega}\right)_{\mathrm{LO}} = \left(\frac{4\pi}{\epsilon_\infty v_0}\frac{\partial\alpha}{\partial\mathcal{E}}\right)^2 \frac{\hbar n_2}{\pi n_1}\left(\frac{\omega_2}{c}\right)^4 \frac{\epsilon_\infty}{8\omega_l}\frac{(\omega_0'^2-\omega_l^2)^2}{(\omega_l^2-\omega_t^2)} . \tag{47}$$

To obtain the integrated TO efficiency we take Eq. (47), use Eq. (22b) for ω_0', with

$$e^{*2} = M\epsilon_\infty v_0(\omega_l^2-\omega_t^2)/4\pi , \tag{48}$$

set $\partial\alpha/\partial\mathcal{E}=0$, and multiply by ω_l/ω_t to obtain the usual result

$$\left(\frac{dR}{d\Omega}\right)_{\mathrm{TO}} = \left(\frac{\omega_2}{c}\right)^4 \frac{n_2}{n_1}\frac{\hbar}{2M\omega_t}\left(\frac{\partial\alpha}{\partial u}\right)^2 \frac{1}{v_0} . \tag{49}$$

For ρ-mechanism scattering from the plasmon in the small damping limit we multiply Eq. (46) by $\frac{1}{2}\omega_p$, use

$$\omega_p^2 = 4\pi ne^2/(m_l^*\epsilon_\infty) , \tag{50}$$

where n is the electron concentration, and where m_l^* is obtained from

$$\frac{m}{m_l^*} = \vec{\eta}_q \cdot \frac{\overleftrightarrow{m}}{m^*}\cdot\vec{\eta}_q , \tag{51}$$

and is the effective mass in the direction of the longitudinal macroscopic field $\mathcal{E}$, and find

$$\left(\frac{dR}{d\Omega}\right)_\rho = \left(\frac{mr_0\omega_2}{m^*\omega_1}\right)^2 \frac{n_2}{n_1}\frac{\hbar q^2}{2m_l^*\omega_p}n . \tag{52}$$

Equations (52) and (46) are consistent with an exact sum rule obeyed by $S(\vec{q},\omega)$, the dynamic form factor for the electron-density operator ρ_q.[20]

---

†Work supported in part by the Advanced Research Projects Agency under Contract No. HC 15-67-C-0221.

*Present address: James Franck Institute, the University of Chicago, Chicago, Ill. 60637.

[1]B. B. Varga, Phys. Rev. 137, A1896 (1965).

[2]K. S. Singwi and M. P. Tosi, Phys. Rev. 147, 658 (1966).

[3]A. Mooradian and G. B. Wright, Phys. Rev. Letters 16, 999 (1966).

[4]A. Mooradian and A. L. McWhorter, in *Light Scattering Spectra of Solids*, edited by G. B. Wright (Springer, New York, 1969), p. 297.

[5]E. Burstein, A. Pinczuk, and S. Iwasa, Phys. Rev. 157, 611 (1967).

[6]J. F. Scott, T. C. Damen, J. Ruvalds, and A. Zawadowski, Phys. Rev. B 3, 1295 (1971).

[7]D. T. Hon, S. P. S. Porto, W. G. Spitzer, and W. L. Faust, in *Spring Meeting Program* (Optical Society of America, Washington, D. C., 1971), p. 38; D. Hon, W. L. Faust, and S. P. S. Porto, Bull. Am. Phys. Soc. 17, 125 (1972).

[8]P. J. Colwell and M. V. Klein, in *Light Scattering in Solids*, edited by M. Balkanski (Flammarion, Paris, 1971), p. 102.

[9]P. J. Colwell and M. V. Klein, Phys. Rev. B 6, 498 (1972).

[10]R. H. Pantell and H. E. Puthoff, *Fundamentals of Quantum Electronics* (Wiley, New York, 1969), Chap. 7.

[11]R. Loudon, Proc. Roy. Soc. (London) A275, 218 (1963); Advan. Phys. 13, 423 (1964); 14, 621 (1965).

[12]J. F. Scott, T. C. Damen, and Jagdeep Shah, Opt. Commun. 3, 384 (1971).

[13]D. W. Feldman, J. H. Parker, Jr., W. J. Choyke, and L. Patrick, Phys. Rev. 173, 787 (1968).

[14]E. N. Foo and N. Tzoar, in Ref. 8, p. 119.

[15]Jack Loader, *Basic Laser Raman Spectroscopy* (Heyden, New York, 1970), pp. 22–24.

[16]S. Singh, J. R. Potopowicz, L. G. Van Uitert, and S. H. Wemple, Appl. Phys. Letters 19, 53 (1971).

[17]J. M. Ralston, R. L. Wadsack, and R. K. Chang, Phys. Rev. Letters 25, 824 (1970).

[18]D. C. Hamilton, Phys. Rev. 188, 1221 (1969); D. L. Mills and E. Burstein, *ibid.* 188, 1465 (1969); R. M. Martin, Phys. Rev. B 4, 3676 (1971).

[19]J. S. Toll, Phys. Rev. 104, 1760 (1956).

[20]D. Pines, *Elementary Excitations in Solids* (Benjamin, New York, 1963), pp. 135, 206.